Self-Tuning Underwater Image Restoration

Emanuele Trucco and Adriana T. Olmos-Antillon

***Abstract*—A self-tuning image restoration filter based on a simplified version of the Jaffe–McGlamery underwater image formation model is presented. Optimal values of the filter parameters are estimated automatically for each individual image by optimizing a quality criterion based on a global contrast measure. The simplified model is ideally suitable for diffuse-light imaging with limited backscatter, but qualitative tests show good performance in a variety of imaging conditions. In addition, quantitative tests with a large number of frames from six real mission videos indicate a substantial performance improvement when restoration is used as a preprocessor for a classifier detecting man-made objects in unconstrained subsea videos.**

***Index Terms*—Computer vision, image restoration, self-tuning systems.**

I. Introduction

THIS paper presents a self-tuning image restoration filter based on a simplified version of the Jaffe–McGlamery underwater image formation model.

Image restoration is, for our purposes, the problem of *recovering a degraded image using quantitative criteria*, i.e., given a model of the degradation and/or of the original image formation. Notice that *image enhancement* usually indicates the same problem but using qualitative or subjective criteria, i.e., nothing is known of the noise or of the image. Restoration techniques appear in the image processing literature under various names in different contexts, including recovery, reconstruction, deblurring, denoizing, deconvolution. [1] and [2] are good introductions, and [3] and [4] recent reviews. Underwater, efficient restoration could improve visualization in real-time and offline inspection of mission videos [5], as well as lead to better results in quantitative image analysis, e.g., automatic classification [6]–[8].

Well-known causes of image degradation underwater include turbidity, particulate matters in the water column, and the interaction between light and medium as light travels through water. All these phenomena are negligible when imaging in air, where the only important effects are due to light sources, surfaces (reflectance characteristics) and sensor properties [9]. Consequently, using full image formation models to design restoration algorithms is more complex in water than in air. In addition, the values of the model parameters relating to water properties, e.g., attenuation and scattering coefficients, are known only approximately in practice.

Given that degradations affect the vast majority of underwater images, one would expect image restoration to feature in many underwater image processing systems. Instead, very few algorithms reported incorporate restoration or explicit imaging models (on this point, see Trucco and Plakas's critical survey of recent subsea video tracking systems [10]). Work addressing image formation in subsea image processing include Li *et al.* [11], who present a detailed photogrammetric model; Eustice *et al.* [12], who adopt enhancement heuristics (e.g., histogram equalization to detect shadows) in a mosaicing system for flow measurement and seafloor mapping; Negahdaripour [13] devises a generalized model to decouple the different changes induced by illumination and motion on image intensities. Liu *et al.* [14] report wavelet-based algorithms for enhancement, detection and tracking in satellite imagery.

Model complexity and uncertainty on parameter values are probably two important reasons discouraging the inclusion of image formation models in image processing algorithms. This paper proposes the design of an image restoration filter tackling the two problems above. First, we devise a simplified version of the well-known, complete underwater image formation model by Jaffe and McGlamery [15], [16]. Our simplifications make a simple design possible. The underlying assumptions point to diffuse illumination and limited backscatter as the ideal imaging conditions for the restoration filter, and experiments indicate good performance even in the presence of significant turbidity. Second, approximate parameter values are used only to initialize the filter; optimal values are estimated by optimizing a quality criterion based on a global contrast measure, guaranteeing that each image is processed by an individually tuned filter.

The main contribution of this paper is therefore the design of a self-tuning restoration algorithm based on the simplified version of the Jaffe–McGlamery model, and its performance assessment with qualitative and quantitative tests. We also give a concise account of the Jaffe–McGlamery model.

The structure of the paper is as follows. Section II reviews the Jaffe–McGlamery model. Section III describes and motivates the simplification of the general model, and uses the results to derive our self-tuning restoration algorithm. Section IV describes briefly the results of our qualitative and quantitative tests. Section V summarizes the main contributions and contents of this paper, and points to future developments.

II. Jaffe–McGlamery Radiometric Model

A. Preliminaries

This section summarizes the Jaffe–McGlamery radiometric model of underwater image formation [15], [16], the basis of our restoration algorithm.

Manuscript received August 2002; accepted July 12, 2004. **Associate Editor: J. J. Leonard.**

E. Trucco is with the Electrical, Electronic and Computer Engineering, School of Engineering and Physical Sciences, Heriot-Watt University, Edinburgh, Scotland EH14 4AS, U.K. (e-mail: e.trucco@hw.ac.uk).

A. T. Olmos-Antillon is with the Electrical, Electronic and Computer Engineering, School of Engineering and Physical Sciences, Heriot-Watt University, Edinburgh, Scotland EH14 4AS, U.K., and the McGill Vision Research, Department of Ophthalmology, Montreal, QC H3A 1A1, Canada (e-mail: adriana.olmos@mcgill.ca).

Color versions of Figs. 3–5 are available online at http://ieeexplore.ieee.org.
Digital Object Identifier 10.1109/JOE.2004.836395

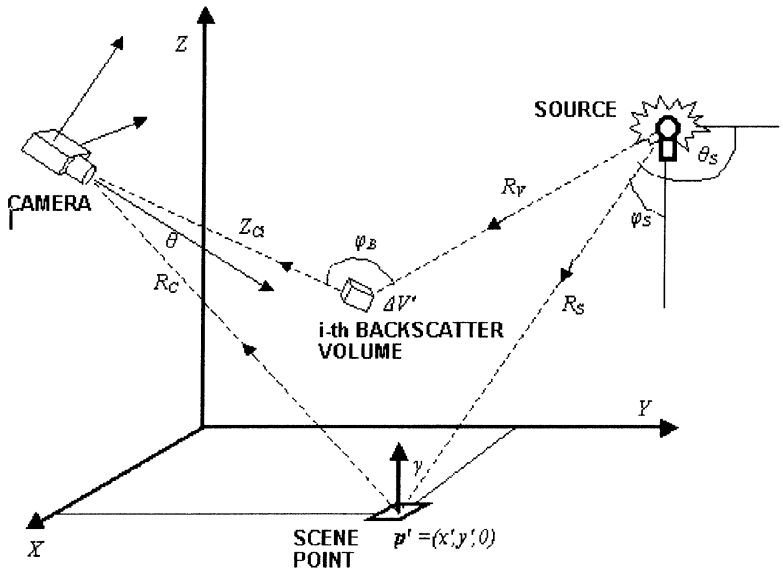

Fig. 1. Essential elements and symbols of the Jaffe–McGlamery model.

Ultimately, the purpose of a radiometric model is to predict the image intensity at each pixel as a function of illumination, reflectance properties of objects, medium, and sensor characteristics. Notice that a key difference between image formation in air and in water is that the interaction between light and medium can be usually ignored in air [9], but produces significant absorption and scattering in water.

McGlamery [15] lays out the theoretical foundations of the model. Jaffe [16] reports extensions and an application to the design of subsea image acquisition systems such that, under reasonably general assumptions, contrast is optimized and backscatter minimized.

The model is developed from two basic facts: linear superposition of effects and medium (water) modeling.

1) Image Formation by Linear Superposition: The irradiance at a specific pixel (point on the image plane) is modeled as the linear superposition of three contributions

- light not reflected by the target scene, or *backscatter* component E_b;
- light reflected directly by the target scene onto the image plane, i.e., not scattered by the intervening water, or *direct component* E_d;
- light reflected by the target scene and scattered by the water by angles small enough that the light still enters the camera, or *forwardscattered component* E_f.

The linear superposition of backscatter, forwardscatter, and direct components generates the *total irradiance* E_T incident on a generic point of the image plane

$$E_T = E_b + E_f + E_d. \tag{1}$$

The purpose of this section is to derive an analytical model for E_T, and, therefore, for E_b, E_f, and E_d.

2) Medium-Light Interactions: Assuming an isotropic, homogeneous medium, the interactions between light and medium (water) modeled in [15] and [16] are attenuation and scattering.

Attenuation is the loss of power as light travels in the medium. It depends on the imaginary part of the complex index of refraction of the medium.

Scattering refers to any deflection from a straight-line propagation path. In the underwater environment, deflections can be due to particles of size comparable to the wavelengths of travelling light (*diffraction*), or to particulate matter with refraction index different from that of the water (*refraction*).

Empirically, the two phenomena can be modeled together by

$$E(\mathbf{p}_2) = e^{-cr} E(\mathbf{p}_1) \tag{2}$$

where $E(\mathbf{p}_2)$ is the irradiance incident on a point $\mathbf{p}_2, E(\mathbf{p}_1)$ is the radiance at a point $\mathbf{p}_1, r$ is the intervening distance, and c is the *total attenuation coefficient*, modeling the removal of light intensity per unit distance and measured by commercially available transmissometers.

In the assumption of an infinitely thin beam (no light scattered back into the beam), attenuation and scattering are separated by modeling c as the sum of two contributions $c = a + b$ referring respectively to absorption and scattering

$$E(\mathbf{p}_2) = e^{-br} e^{-ar} E(\mathbf{p}_1). \tag{3}$$

3) Section Roadmap: The remainder of this section is divided in two parts. First, analytical expressions are formulated for the effects of illumination, object reflectance and camera. Second, such expressions are brought together to model the three components in (1), leading to a complete model for E_T.

B. Modeling Illumination, Reflectance, and Camera

1) Illumination: Assume a point source characterized by a given beam pattern, defined by a function $b(\theta_s, \varphi_s)$. This function expresses the irradiance received by a unit surface on a hemispherical shell at unit distance from the source, in watt per square meter. The angles θ_s, φ_s (Fig. 1) define the direction of the ray from the source to a point $\mathbf{p}'$, center of a differential, planar patch on the scene surface. This point is described in a

reference frame X, Y, Z fixed to the scene, and chosen so that $\mathbf{p}'$ lies on the plane $z = 0$; therefore, $\mathbf{p}' = (x', y', 0)$.

Before reaching the scene, the beam pattern spreads spherically and is attenuated by the water. Therefore the irradiance incident on the scene at $\mathbf{p}'$ can be written as

$$E'_I(\mathbf{p}') = \cos\gamma \frac{e^{-cR_s}}{R_s^2} b(\theta_s, \varphi_s) \tag{4}$$

where γ is the angle formed by the ray incident on the scene at $\mathbf{p}$ and the normal to the scene surface at $\mathbf{p}$. R_s is the distance between $\mathbf{p}$ and the source. Fig. 1 illustrates the variables involved.

Some of the irradiance reaching the surface is due to forward scattering, in the small-angle assumption. To include this, (4) becomes

$$E_I(\mathbf{p}') = E'_I(\mathbf{p}') * g(x', y', R_s, G, c, B) + E'_I(\mathbf{p}') \tag{5}$$

where $*$ indicates convolution, and g is a point-spread function defined by

$$g(x', y', R_s, G, c, B) = \left[e^{-GR_s} - e^{-cR_s}\right] \mathcal{F}^{-1}\left\{e^{-BR_s\omega}\right\}. \tag{6}$$

Here, G is an empirical constant such that $|G| < |c|$, B is a damping function determined empirically, $\mathcal{F}^{-1}$ indicates inverse Fourier transform, and ω is the radial frequency. This model has been proven empirically valid in the small-angle scattering approximation [16].

2) Object Reflectance: Here, the problem is to determine how much of the irradiance incident on a specific $\mathbf{p}'$ on the scene surface is reflected, and with which spatial distribution. The model summarizes surface reflectance in a *planar reflectance map*, $M(x', y')$, essentially an attenuation coefficient. Typical values in oceanic waters range between 0.02 and 0.1 [16]. Notice that $M(x', y')$ and (4) lead to a model reminiscent of Lambert's law [9]: $\cos\gamma$ is the Lambertian cosine term, and M replaces the constant albedo.

3) Camera: Three attenuations are modeled which make the irradiance on the image plane less than the radiance entering the camera. The first is a *peripheral attenuation* due to the optics (basically the presence of a finite aperture), modeled by a term $(\cos^4\theta)/(F)$, where θ is the angle formed by the incoming ray with the optical axis of the camera, and F is the F-number of the lens [9]. The second is due to the *lens transmittance*, and modeled by a multiplicative coefficient, T_l. The third depends on the *relative values of focal length*, F_l, *and stand-off distance*, R_c. The total attenuation of light entering the camera, before reaching the image plane, is, therefore, captured by the multiplicative coefficient

$$\frac{T_l \cos^4\theta}{F}\left[\frac{R_c - F_l}{R_c}\right]. \tag{7}$$

C. Complete Model for Image Irradiance

We shall now use the expressions referring to illumination, reflectance, camera, and medium to arrive at expressions for E_b, E_f, and E_d, and hence, to a complete model for E_T in (1).

1) Direct Component: E_d in (1) can be written as a function of the irradiance E_I on the scene surface at a point $\mathbf{p}'$. It must, therefore, account for the reflectance of the surface, the attenuation through the medium, and the effect of the camera. Using results from Section II-B2 and B3

$$E_d(x, y) = \left\{M(\mathbf{p}')e^{-cR_c}\frac{T_l\cos^4\theta}{F}\left[\frac{R_c - F_l}{R_c}\right]\right\} E_I(\mathbf{p}') \tag{8}$$

where R_c is the stand-off distance from $\mathbf{p}'$ to the camera.

2) Forwardscattered Component: E_f in (1) is modeled as done in (5) in the small-angle assumption

$$E_f = E_d * g(x, y, R_c, G, c, B). \tag{9}$$

3) Backscatter Component: The small-angle approximation does not hold for the computation of E_b in (1). Here, the model must take into account light contributions from a large volume of water between scene and camera. The reasoning is as follows:

1) divide the intervening volume into thin, planar slabs parallel to the image plane, each at distance Z_{ci} from the camera and R_V from the illumination source;
2) compute the irradiance on each slab due to direct and forwardscattered light;
3) compute E_b as linear superposition of the light contributions from all slabs, weighted by a suitable volume-scattering function.

The irradiance on a differential volume $\Delta V'$ is, according to point 2 above, $E_s = E_{s,d} + E_{s,f}$, where

$$E_{s,d} = \frac{e^{-cR_V}}{R_V^2} b(\theta_i, \varphi_i) \tag{10}$$

$$E_{s,f} = E_{s,d} * g(\Delta V', R_c, G, c, B). \tag{11}$$

The resulting radiant intensity scattered toward the camera by $\Delta V'$ is

$$H_b = \beta(\varphi_b) E_s \Delta V'$$

where $\beta(\varphi_b)$ is the volume scattering function, and φ_b (Fig. 1) is the angle formed by the irradiance and radiance rays at $\Delta V'$.

The image due to the radiant intensity from $\Delta V'$ is then calculated considering the direct component

$$E_{b,d} = \sum_{i=1}^{N} e^{-cZ_{ci}} \frac{\pi \Delta Z_i}{4F^2} \cos^3\theta T_l \left[\frac{Z_{ci} - f_l}{Z_{ci}}\right]^2 \frac{H_b}{\Delta V'}. \tag{12}$$

Finally, the calculation of E_T is completed by modeling E_b. Once again, the irradiance E_b incident on an image point and due to backscatter is calculated by simulating an additive forwardscattered component

$$E_b = E_{b,d} + E_{b,d} * g(\mathbf{p}, R_c, G, c, B). \tag{13}$$

III. Adaptive Underwater Image Restoration

The Jaffe–McGlamery model covers a wide spectrum of imaging conditions, and as such results in a complex numerical

TABLE I
TYPICAL PARAMETER VALUES IN THE INVERSE FILTERING PROCESS

Variable	*Ranges*
K (weight constant)	0.9 - 0.2
c (attenuation coefficient)	water type (m^{-1}) 0.323 bay 0.252 coastal 0.049 deep ocean
R_c (depth)	order of meters
Fl (focal length)	.035 m (typical value)

model difficult to use for filter design. This section aims to introduce simplifications suitable for designing a simple and efficient restoration filter. This reduces generality but still accounts for a sufficiently wide class of practical situations, as discussed later. In addition, as parameter values are seldom known in real situations, a contrast-based optimization tunes the filter parameters to the best estimated values for the image under examination.

A. Specializing the Model for Filter Design

We assume no *a priori* information on the imaging conditions, apart from an approximate knowledge of the model as discussed in Section III-B. We therefore consider the illumination uniform, which seems reasonable in shallow waters, where illumination is provided by direct sunlight.

We do not consider the explicit expression of the backscatter component E_b the part of the model less likely to lead efficiently to a restoration filter. Instead, we consider only the forwardscattered component, E_f, and simplify the model as discussed later. This appears reasonable whenever the concentration of particulate matter generating backscatter in the water column is limited.

A further simplification is to consider the difference of exponentials in the forwardscatter model (9) and (6) an experimental constant, as variation is limited in most practical cases

$$K \sim [e^{-GR_c} - e^{-cR_c}]. \tag{14}$$

Typical values for K are shown in Table I.

Finally, we concentrate on forward scattering as the major degradation source, ignoring the detailed parametrization of the direct component. In other words, we aim to combat forward scattering as the main corrupting effect, and focus the model on it. In a similar spirit, Zhang and Negahdaripour [17] point out that backscatter, not carrying information about the scene, should be minimized by designing an adequate imaging system, and mention polarization, volume scanning and range gating as possible examples.

Our assumptions point to low-backscatter, shallow-water conditions as the optimal environment for our technique. However, experiments indicate that the technique may bring some improvements even with considerable backscatter (Section IV).

The assumptions discussed make it possible to design a simple inverse filter in frequency domain. The Fourier transform of the resulting, simplified imaging model is simply

$$G(f, R_c, c, K) = Ke^{-BR_c\omega} \tag{15}$$

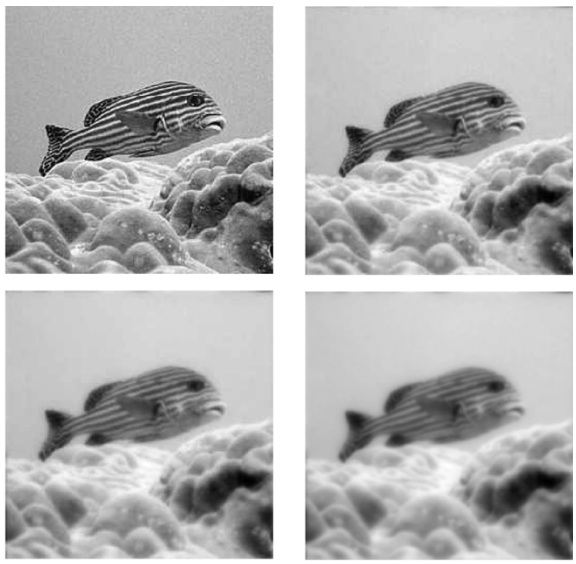

Fig. 2. Examples of simulated image degradations using the simplified model on a real image near-perfect focus (top left). In this example, c $= .045$ m^{-1}, K $= 0.7$. Camera-scene distance: (top right) $R_c = 12$ m, (bottom left) 22 m, (bottom right) 32 m. Original image courtesy of Peter Hince, Ocean Images, U.K. (www.oceanimages-uk.com).

but B is well approximated by c in situations of practical interest, so that we can write

$$G(f, R_c, c, K) \approx Ke^{-cR_c\omega}. \tag{16}$$

Examples of simulated degradations using the simplified model, in essence a low-pass filter, are shown in Fig. 2.

The inverse filter is now simply

$$\frac{1}{G(f, R_c, c, K)} = \frac{1}{K}e^{cR_c\omega}. \tag{17}$$

The next problem is the choice of parameter values leading to good results with each image. Obviously, one cannot rely on manual parameter selection in real applications, in which high volumes of images are processed. Examples include post-mission analysis of video data and online processing of video streams acquired by a ROV or AUV. For this reason, we introduce a self-tuning strategy.

B. A Self-Tuning Restoration Filter

The key problem is that useful values of the filter's parameters are not known in advance, or are known only approximately and vary in different images. Hence we incorporate optimal parameter estimation within the filtering process itself. We consider a cost function quantifying the difference between the current, filtered image and the ideal, undegraded version. The parameter vector leading to the filtered image which minimizes this cost identifies the optimal filter. As the ideal image is of course unknown, we estimate the difference using a global measure of blur. This makes sense as the main degradation predicted by (16) is an attenuation of high frequencies.

Several measures of blur have been proposed in the computer vision literature [18], [19]. They basically quantify the amount

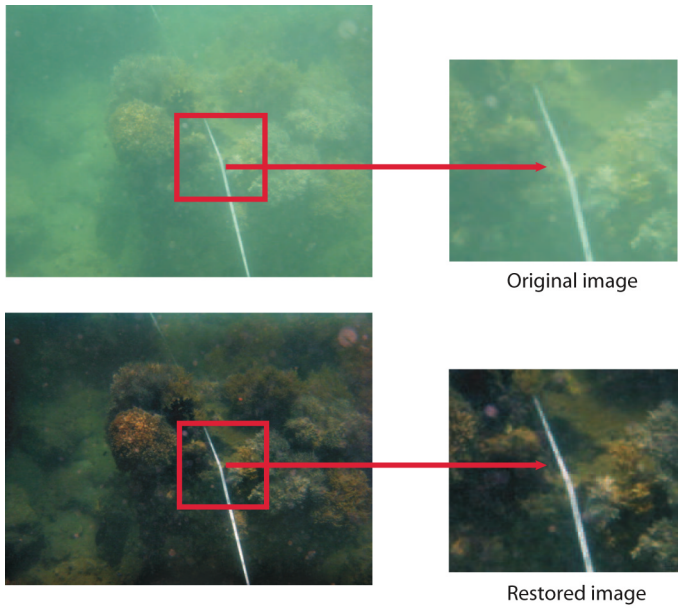

Fig. 3. Example of restoration, with enlarged detail. Top row: input image. Bottom row: restored image. Initial parameter values: $K = 0.7, c = 0.045\ \mathrm{m}^{-1}, F_l = 35$ cm. Final parameter values: $K = 0.90, c = 0.045\ \mathrm{m}^{-1}$. Original image courtesy of Franck Magron, Secretariat of the Pacific Community.

of texture or the high-frequency contents in small neighborhoods of each pixel. We found experimentally that the *Tenengrad*, in essence the average squared gradient magnitude, makes an adequate cost function for our purposes

$$T = \sum_{W(\mathbf{p})} \sum \|\nabla I(\mathbf{p})\|^2 \tag{18}$$

where W is a small neighborhood of an image point $\mathbf{p}$ and I is the pixel's intensity. We estimate the gradient magnitude with a simple Sobel filter [9].

The optimization determining the optimal filter parameters is performed by a Nelder–Mead simplex search determined from typical values known to apply in relevant oceanic conditions (see Table I). R_c ranged between 1 and 20 m approximately in our experiments.

For clarity, we conclude this section with a concise statement of the overall algorithm

1) initialize parameters to expected values for chosen water conditions;
2) acquire frame;
3) apply restoration filter (17) with current parameter values, and estimate image quality using (18);
4) optimize image quality using (in our case) a Nelder–Mead technique, identifying optimal values for the restoration parameters;
5) return optimal parameter values.

IV. Experimental Results

This section summarizes two types of experiments: qualitative assessment of the restoration quality by visual inspection, and quantitative performance analysis using the restoration filter as preprocessor for a classifier.

The system was implemented in MATLAB and tested on a Linux PC (Pentium III, 733 MHz). The current optimization algorithm is not designed for speed, and the determination of the optimal parameters may take up to a minute per frame. However the MATLAB restoration does not take longer than 3.8 s (worst case measured) with 320×240 images. Experience from previous developments (e.g., [20]) suggests that an optimized C version could arguably run at several frames per second on a state-of-the-art PC.

Fig. 4. Top row: input image. Bottom row: restored image. Initial parameter values: $K = 0.7, c = 0.045\ \mathrm{m}^{-1}, F_l = 35$ cm. Final parameter values: $K = 0.73, c = 0.048\ \mathrm{m}^{-1}$. Original image acquired during GOATS trials 2000, Elba, Italy.

A. Qualitative Assessment

Figs. 3–5 are examples of good-quality results achieved when imaging conditions are close to the assumptions of the simplified model: absorption can be significant (e.g., Fig. 5, but

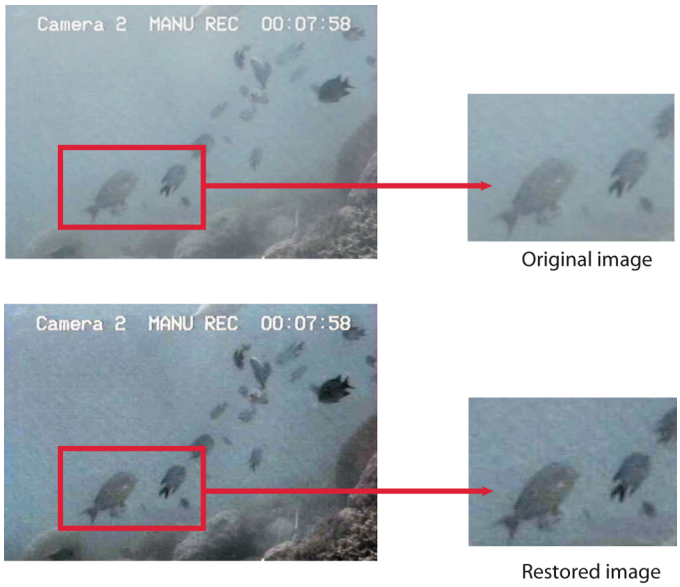

Fig. 5. Example of restoration, with enlarged detail. Top row: input image. Bottom row: restored image. Initial parameter values: $K = 0.7, c = 0.045$ m^{-1}, $F_l = 35$ cm. Final parameter values: $K = 0.92, c = 0.0448$ m^{-1}. Original image courtesy of Franck Magron, Secretariat of the Pacific Community.

backscatter must be limited. In this case, the filter gave good results systematically.

Fig. 6 is an example of the very limited benefits introduced when backscatter becomes the preponderant effect, and the data seriously degraded.

B. Quantitative Assessment

We assessed quantitatively the benefits of the self-tuning filter as a preprocessor for image classification. This is similarly to what Shin *et al.* have done [21] on the comparison of edge detectors using an object recognition task. The hypothesis was that better classification results would be achieved with restored imagery than with unprocessed ones.

The classifier used was our contour-based, two-class system detecting the presence of generic man-made objects in unconstrained subsea sequences. In other words, images are classified as containing or not containing man-made objects. We sketch here the key points of the algorithm for completeness, but refer the reader to [22], [23] for details. First, given an input image, the system determines an optimal scale for contour extraction. Second, contours are extracted and ranked according to measures inspired by perceptual organization [24], and capturing general properties of man-made artifacts. Third, the ranked contours are input to a suitably trained support vector machine (SVM) algorithm [25], which generates the final answer. An important SVM parameter for our explanation is the *bias*, i.e., the distance from the origin of the optimal separating hyperplane.

We used six real videos, two for training and four for testing. The training videos were acquired during shallow-water AUV trials run by Florida Atlantic University (FAU), Fort Lauderdale, covering a variety of imaging conditions. We selected manually 342 frames, of which 171 contained man-made objects and 171 contained only natural background. Of the four test videos, one

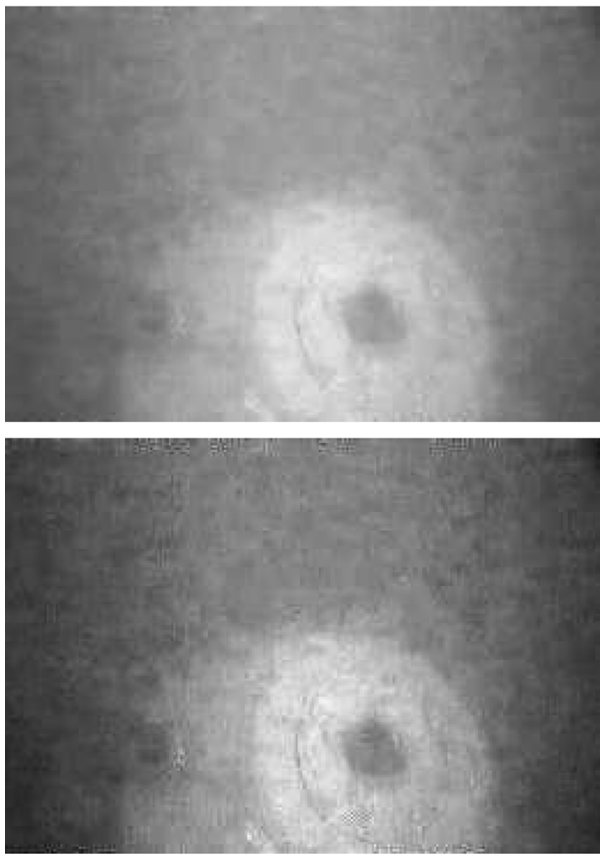

Fig. 6. Example of restoration with an image acquired in conditions not meeting the model's assumptions (high backscatter); the visual improvement is marginal. Initial parameter values: $K = 0.7, c = 0.045$ m^{-1}, $F_l = 35$ cm. Final parameter values: $K = 0.951, c = 0.0406$ m^{-1}. Original image courtesy of Florida Atlantic University.

was acquired in our own instrumented tank, two during further AUV trials in turbid-water conditions run by FAU and Camp Pendleton, San Diego, CA, and one during GOATS trials in 2000

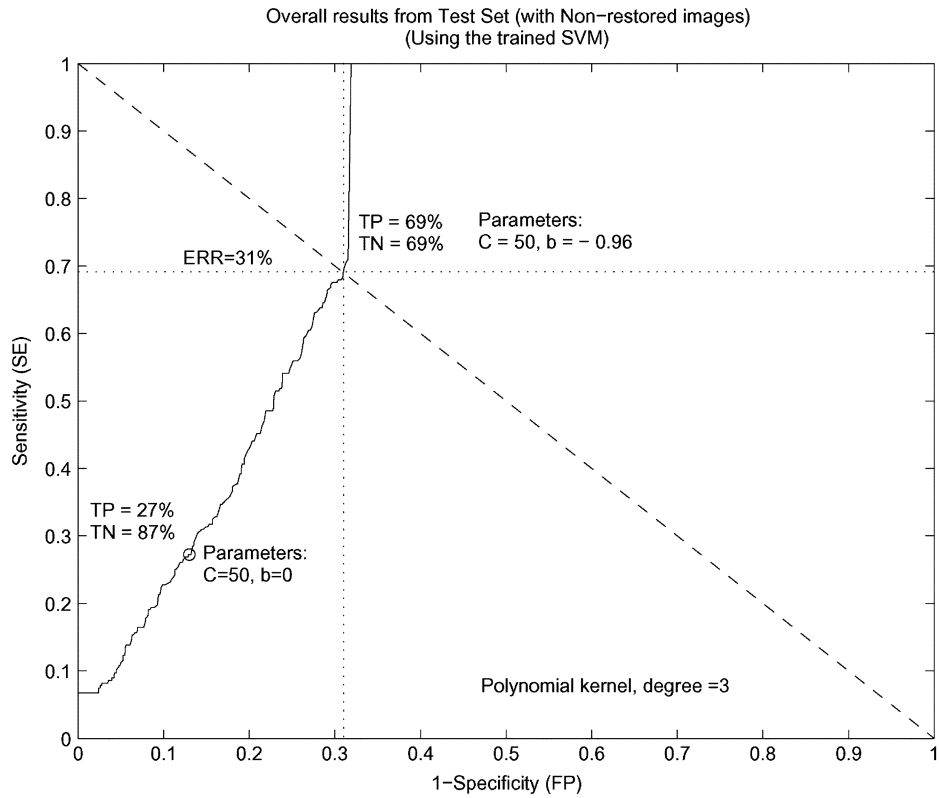

Fig. 7. ROC curve of classification test with unrestored image sets.

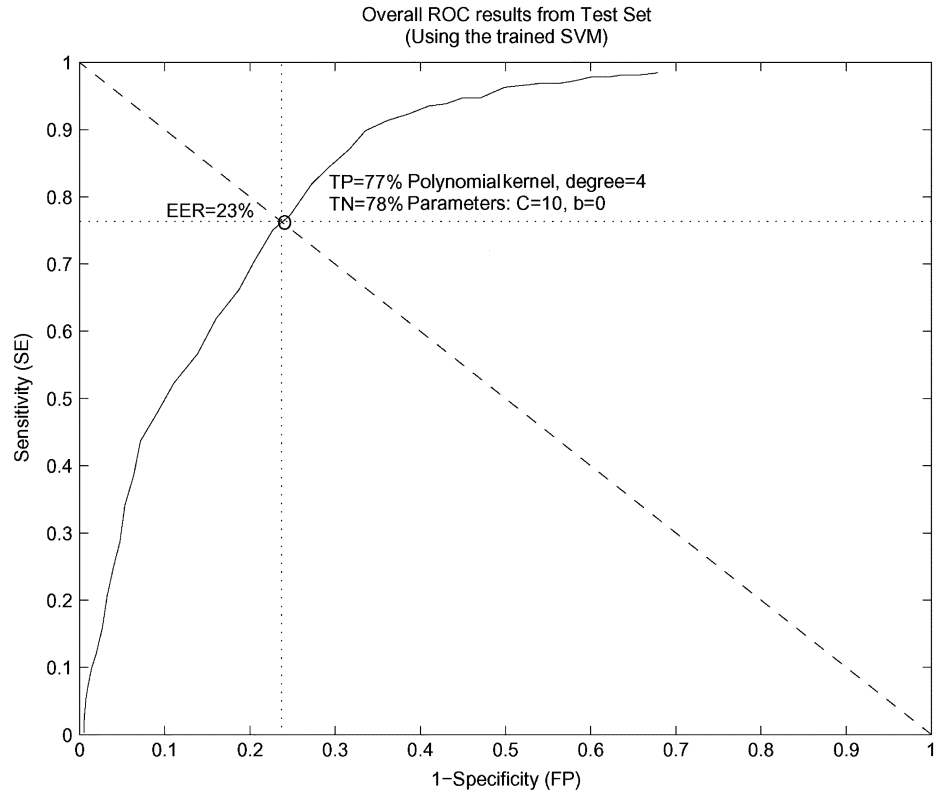

Fig. 8. ROC curve of classification test with restored image sets.

off the coast of Elba Island (Italy). We digitized the videos at a common rate of ten frames per second. The complete testing set consisted of 1806 frames. The images were ground-truthed manually, by visual inspection.

Our restoration filter was run on the training and the test sets. The classifier was then trained and run, first on the unprocessed sets, then on the restored sets. We report results in terms of ROC curves [26], a compact visualization of the tradeoff between the amounts of false positives (sensitivity S_e) and true positives (specificity S_p). As a brief reminder, $S_e = \mathrm{TP}/(\mathrm{TP}+\mathrm{FN})$, and $S_p = \mathrm{TN}/(\mathrm{TN}+\mathrm{FP})$, where the symbols spans the combinations of "true, false" and "positives, negatives." The curve is parametrized (indexed) by a classification parameter of choice, in our case the bias of the SVM. The closer the curve to the top-left corner $(S_p = 0, S_e = 1)$, the closer the performance to the ideal case (output contains only true positives/negatives, no false positive/negative). In practice, the curve runs at some distance from the ideal lines and the point of optimal performance, or *equal error rate* (ERR), is defined as the best compromise between FP anf TP. This is achieved at the intersection of the ROC curve with the line $S_p = 1 - S_e$. The smaller the ERR, the better the classifier.

Fig. 7 shows results with the unprocessed training and test sets. The curve is parametrized by the bias parameter of the SVM classifier [22]. Here, the true positives (images containing man-made objects and classified as such) were 69%; the true negatives (image not containing man-made objects and classified as such) were also 69%. The ERR was 31%. For b less than -0.96, the classification results remained constant, hence the vertical segment. When the classifier was run on the restored sets (Fig. 8), the TP and TN percentages became, respectively, 77% and 78%, with an improved ERR equal to 23%. The shape of the graph in itself suggests better performance. This result supports the hypothesis that our restoration algorithm can improve classification. As a final note, the apparently low percentages of TP and TN must be interpreted in the context of the very general problem considered (detection of generic man-made objects in unconstrained videos).

Finally, we would like to mention that some of these test videos and still images can be found online at http://emfs1.eps.hw.ac.uk/~ceeet1/Restoration/.

V. Conclusion

This paper has presented a self-tuning restoration filter based on a simplification of the general Jaffe–McGlamery underwater image formation model, and a concise account of the latter. The simplified model is ideally suitable for shallow-water, diffuse-light conditions with limited backscatter, but experimental results suggest that useful enhancement is achieved in a variety of imaging conditions. The algorithm presented is self-tuning, in the sense that optimal parameter values are estimated for each image. Optimality is defined as achieving minimum blur, measured by the Tenengrad criterion. Quantitative tests with a large number of frames from real-mission videos reveal a substantial, quantitative improvement to an important classification task for subsea operations, detecting man-made objects on the seafloor.

Future work includes tracking parameter values over time (at the moment, each frame is treated independently), including a more efficient, problem-specific optimization algorithm, investigating alternative cost functions incorporating further image quality measures, and using the temporal evolution of the estimated parameters for automatic segmentation of video sequences, in the spirit of [27].

References

[1] R. C. Gonzalez and R. E. Woods, *Digital Image Processing*. Reading, MA: Addison-Wesley, 1992.

[2] M. Petrou and P. Bosdogianni, *Image Processing: The Fundamentals*. New York: Wiley, 1999.

[3] M. R. Banham and A. K. Katsaggelos, "Digital image restoration," *IEEE Signal Process. Mag.*, vol. 14, no. 2, pp. 24–41, Mar. 1997.

[4] P. Kornprobst, R. Deriche, and A. Gilles, "Estimation of autoregressive signals from noisy measurements," in *Proc. IEEE Int. Conf. Comp. Vis. Pattern Recog. (CVPR97)*, 1997, pp. 325–330.

[5] K. Lebart, E. Trucco, and D. M. Lane, "Real-time automatic sea-floor change detection from video," in *Proc. MTS/IEEE Conf. OCEANS 2000*, 2000, pp. 337–343.

[6] G. L. Foresti and S. Gentili, "A hierarchical classification system for object recognition in underwater environments," *IEEE J. Ocean. Eng.*, vol. 27, no. 1, pp. 66–78, Jan. 2002.

[7] S. Reed, Y. R. Petillot, and J. M. Bell, "An automatic approach to the detection and extraction of mine features in sidescan sonar," *IEEE J. Ocean. Eng.*, vol. 28, no. 1, pp. 90–105, Jan. 2003.

[8] D. M. Kocak, N. da Vitoria Lobo, and E. A. Widder, "Computer vision techniques for quantifying, tracking, and identifying bioluminescent plankton," *IEEE J. Ocean. Eng.*, vol. 24, no. 1, pp. 81–95, Jan. 1999.

[9] E. Trucco and A. Verri, *Introductory Techniques for 3-D Computer Vision*. Englewood Cliffs, NJ: Prentice-Hall, 1998, pp. 97–100.

[10] E. Trucco and K. Plakas, "Video tracking: A concise survey," *IEEE J. Ocean. Eng.*, vol. 31, no. 2, pp. 520–529, Apr. 2006.

[11] R. Li, H. Li, W. Zou, R. Smith, and T. Curan, "Quantitative photogrammetric analysis of digital underwater video imagery," *IEEE J. Ocean. Eng.*, vol. 22, no. 2, pp. 364–375, Apr. 1997.

[12] R. Eustice, H. Singh, and J. Howland, "Image registration underwater for fluid flow measurements and mosaicking," in *Proc. MTS/IEEE Conf. OCEANS 2000*, vol. 3, 2000, pp. 1529–1534.

[13] S. Negahdaripour, "Revised definition of optical flow: Integration of radiometric and geometric cues for dynamic scene analysis," *IEEE Trans. Pattern Anal. Mach. Intell.*, vol. 20, no. 9, pp. 961–979, Sep. 1998.

[14] A. C. Liu, C. Y. Peng, and S. Y.-S. Chang, "Wavelet analysis of satellite images for coastal watch," *IEEE J. Ocean. Eng.*, vol. 22, no. 1, pp. 9–17, Jan. 1997.

[15] B. L. McGlamery, "A computer model for underwater camera systems," in *SPIE Ocean Optics*, vol. 208, 1979, pp. 221–231.

[16] J. S. Jaffe, "Computer modeling and the design of optimal underwater imaging systems," *IEEE J. Ocean. Eng.*, vol. 15, no. 2, pp. 101–111, Apr. 1990.

[17] S. Zhang and S. Negahdaripour, "3-d shape recovery of planar and curved surfaces from shading cues in underwater images," *IEEE J. Ocean. Eng.*, vol. 27, no. 1, pp. 100–116, Jan. 2002.

[18] E. Krotkov, "Focusing," *Int. J. Comput. Vision*, vol. 1, pp. 223–237, 1987.

[19] S. K. Nayard and Y. Nakagawa, "Shape from focus," *IEEE Trans. Pattern Anal. Mach. Intell.*, vol. 16, no. 8, pp. 824–831, Aug. 1994.

[20] C. Plakas and E. Trucco, "Developing a real-time, robust, video, tracker," in *Proc. MTS/IEEE Conf. OCEANS 2000*, Sep. 2000, pp. 1345–1352.

[21] M. C. Shin, D. Goldgof, and K. W. Bowyer, "Comparison of edge detectors using an object recognition task," in *IEEE Proc. Comput. Vision Pattern Recog.*, 1999, pp. 360–365.

[22] A. Olmos and E. Trucco, "Detecting man-made objects in unconstrained subsea videos," in *Brit. Mach. Vision Conf.*, 2002, pp. 517–526.

[23] A. Olmos, E. Trucco, and D. Lane, "Automatic man-made object detection with intensity cameras," in *Proc. MTS/IEEE Conf. OCEANS 2002*, vol. 3, Oct. 2002, pp. 1551–1561.

[24] D. G. Lowe, *Perceptual Organization and Visual Recognition*. Norwell, MA: Kluwer, 1985.

[25] N. Cristianini and J. Shawe-Taylor, *An Introduction to Support Vector Machines and Other Kernel-Based Learning Methods*. Cambridge, U.K.: Cambridge Univ. Press, 2000.

[26] K. Bowyer, C. Kranenburg, and S. Doughert, "Edge detector evaluation using empirical roc curves," in *Proc. IEEE Int. Conf. Comput. Vision Pattern Recog. (CVPR99)*, 1999, pp. 354–359.

[27] K. Lebart, C. Smith, E. Trucco, and D. M. Lane, "Automatic indexing of underwater survey video: algorithm and benchmarking method," *IEEE J. Ocean. Eng.*, vol. 28, no. 4, pp. 673–686, Oct. 2003.

Emanuele Trucco received the B. Sc. and Ph.D. degrees in electronic engineering from the University of Genoa, Genoa, Italy, in 1984 and 1990, respectively.

Currently, he is a Reader (Associate Professor) in the School of Engineering and Physical Sciences, Heriot-Watt University, Edinburgh, U.K. He published more than 100 refereed publications and co-authored (with Alessandro Verri) a book widely adopted by the international community. Press reports include *New Scientist*, the *Financial Times*, and an invited participation in the BBC *Tomorrow's World Roadshow* 2002. His research interests are in multiple view vision, motion analysis, image-based rendering, and applications to image-based communications, videoconferencing, medical image processing and subsea robotics.

Dr. Trucco has served as and Editor of the IEEE TRANSACTIONS ON SYSTEMS, MAN, AND CYBERNETICS (PART C) and an Honorary Editor of the IEE Proceedings in Vision, Signal and Image Processing, and Pattern Analysis and Applications. He has received research funding and awards from the European Union, EPSRC, various foundations such as Royal Society and British Council. He serves regularly on professional, technical, and organizing committees for international events in computer vision and image processing.

Adriana T. Olmos-Antillon received the Diploma in electrical engineering and telecommunication from the Universidad Iberoamericana Leon, Guanajuato, Mexico, in 1998, and the Ph.D. degree in electronic engineering from Heriot-Watt University, Edinburgh, U.K., in 2002.

Since then, she joined the McGill Vision Research Laboratory, Montreal, QC, Canada, as a Postdoctoral Research Fellow. Her current research interests are centred around the areas of color vision, image processing, and pattern recognition.